Available online at www.sciencedirect.com
SCIENCE DIRECT
Catalysis Today 114 (2006) 422–427
CATALYSIS TODAY
www.elsevier.com/locate/cattod

Structural changes and activation treatment in a Co/SiO_2 catalyst for Fischer–Tropsch synthesis

V.A. de la Peña O'Shea [a,b,*], N. Homs [a], J.L.G. Fierro [b], P. Ramírez de la Piscina [a,**]

[a] *Departament de Química Inorgànica, Universitat de Barcelona. C/ Martí i Franquès 1-11, 08028 Barcelona, Spain*
[b] *Instituto de Catálisis y Petroleoquímica, CSIC, Campus Cantoblanco, 28049 Madrid, Spain*

Available online 18 April 2006

Abstract

We examined the effect of the activation process on the structural and morphological characteristics of a cobalt-based catalyst for Fischer–Tropsch synthesis. A 10 wt.% Co/SiO_2 catalyst prepared by wet impregnation was separately activated under H_2, CO or a H_2/CO mixture. The structural changes during activation from 298 to 773 K were studied by in situ X-ray diffraction. Catalysts were examined by SEM, TEM, XPS and in situ DRIFT-MS. The H_2/CO activation produced redispersion of cobalt particles and simultaneous carbon nanostructures formation. The catalyst showed the highest performance in the Fischer–Tropsch synthesis after the H_2/CO activation.

Keywords: Cobalt catalyst; Fischer–Tropsch; Syngas activation; In situ XRD; In situ DRIFT

1. Introduction

Nowadays, the Fischer–Tropsch synthesis (FTS) is one of the most attractive processes to alternatively obtain raw products for lubricants and clean diesel fuels from syngas. Although several metals catalyse this well-known reaction, cobalt-based catalysts are widely used because of their higher activity/price ratio, selectivity and stability [1–3].

Highly dispersed metallic cobalt activates carbon monoxide and hydrogen, and supported cobalt catalysts have been used successfully in industrial-scale FTS processes [4–7]. However, the behaviour of cobalt-based catalysts in the FTS reaction depends on several parameters, such as support characteristics and promoter addition [8–11]. Moreover, the characteristics and properties of the surface active species strongly depend on the preparation method and, especially for the supported systems, on the calcination conditions, which in turn control the active phase–support interaction [12–15].

The catalytic performance of cobalt-based systems in FTS depends directly on the number and availability of active sites [15,16]. The calcined catalyst precursor is usually activated in a reducing atmosphere to obtain a metallic cobalt phase (Co^0). Depending on the composition of the reducing atmosphere and the temperature of the activation, different cobalt-containing phases can be obtained which in turn affect the catalytic properties of the material. Thus, besides Co^0, different phases of cobalt carbides and oxides can be obtained when H_2, CO or $H_2 + CO$ mixture (syngas) are used. The transformation of metallic cobalt species to cobalt carbides and/or oxides in FTS conditions has also been reported [17–19].

In a previous study, the catalytic activity of a silica-supported cobalt catalyst was strongly enhanced when activation was carried out under $H_2 + CO$ (1/1). In addition, unsaturated products were almost completely inhibited [20]. Here we examine the effect of the activation conditions on the structural changes and catalytic properties of silica-supported cobalt catalysts. Hydrogen, carbon monoxide or syngas atmospheres were used to activate the calcined catalyst precursors. Structural changes during the treatment were followed by in situ X-ray diffraction, and samples were characterized before and after treatment by X-ray photoelectron spectroscopy, scanning electron microscopy and transmission electron microscopy. In situ diffuse reflectance infrared spectroscopy coupled to on-line mass spectrometry, to monitor the FTS products, was used to identify surface species under activation conditions and to perform in situ CO chemisorption experiments.

* Corresponding author. Tel.: +34 934021235; fax: +34 934907725.
** Corresponding author. Tel.: +34 934037056; fax: +34 934907725.
E-mail addresses: victor@qi.ub.es (V.A. de la Peña O'Shea), pilar.piscina@qi.ub.es (P. Ramírez de la Piscina).

0920-5861/$ – see front matter © 2006 Elsevier B.V. All rights reserved.
doi:10.1016/j.cattod.2006.02.065

2. Experimental

2.1. Preparation of catalysts

A silica-supported cobalt catalyst (Co = 10 wt.%) was prepared by wet impregnation of a silica carrier (Grace Davison, 299 m^2/g) with an aqueous solution of cobalt nitrate ($Co(NO_3)_2{\cdot}6H_2O$). Solid was dried at 393 K overnight and calcined at 773 K under flowing air for 2 h (Co10-c sample). Different portions were then separately activated under H_2, CO or a H_2/CO (1/1) mixture from 498 to 773 K. Catalysts were labelled Co10–H_2, Co10–CO or Co10–H_2 + CO depending on the activation process.

2.2. Characterisation of catalysts

The cobalt content of the catalyst after calcination was determined by inductively coupled plasma using Perkin-Elmer Optima 3300 DV equipment.

A powder X-ray diffraction (XRD) in situ study was carried out during the different activation processes. XRD patterns were recorded with a D500 Siemens diffractometer, using nickel-filtered Cu $K\alpha_1$ radiation ($\lambda = 0.15406$ nm). XRD profiles were collected in the 2θ angle between 34° and 54°, at a step width of 0.1° and by counting 5 s at each step. The reactor cell was an ANTON PAAR with a sample holder of laminate platinum. Samples were heated from 298 to 773 K (5 K min^{-1}) under H_2, CO or H_2/CO (1/1) flow (40 ml min^{-1}). Temperature was measured by a thermocouple in contact with the sample holder.

Scanning electron microscopy (SEM) was carried out with a microscope ISI DS-130 coupled to a solid-state detector Si/Li Kevex and a SUN SparcStation 5 for acquiring and processing energy-dispersive X-rays (EDX) spectra.

Transmission electron micrographs (TEM) were taken with a Fei Tecnai G30 microscope. The acceleration voltage was set at 200 kV. The powdered samples were deposited on copper grids covered with fine carbon films from acetone suspensions.

X-ray photoelectron spectra (XPS) were acquired with a Fisons ESCALAB MkII 200R spectrometer equipped with a hemispherical electron analyser and an Al Kα ($h\nu = 1486.6$ eV, 1 eV = 1.6302×10^{-19} J) 120 W X-ray source. All binding energies (BE) were referenced to the adventitious Si 2p line at 103.4 eV. This reference gave BE values within an accuracy of ± 0.2 eV. Atomic ratios were computed from the intensity ratios normalized by atomic sensitivity factors [21].

For in situ infrared experiments, about 20 mg of catalyst was placed in a Spectra Tech catalytic chamber on a Nicolet Magna 750 infrared spectrometer, operating in diffuse reflectance mode (DRIFT). H_2, CO or syngas were introduced into the DRIFT chamber by means of mass-flow controllers. The outlet of the DRIFT chamber was connected on-line through a capillary tube held at 423 K to a Balzers QMS200 instrument equipped with a quadrupole mass spectrometer. Several mass values were selected and previously calibrated in the apparatus in order to monitor the evolution of different products (hydrogen, carbon oxides, C_1–C_4 hydrocarbons).

3. Results and discussion

Preliminary characterization of Co10-c (calcined sample) has already been reported [22]. The XRD pattern indicated the sole presence of Co_3O_4 cubic phase with a crystallite average size determined using the Scherrer equation of 21 nm. The surface analysis was performed by XPS. From the analysis of Co $2p_{3/2}$ level, the presence of Co^{3+} (Octahedral) and Co^{2+} (Tetrahedral) was deduced with a Co^{3+}/Co^{2+} ratio of 76/24. This is consistent with the presence of Co_3O_4 on the surface of the catalyst [23–26], the Co_3O_4 particles having an excess of oxygen in the surface that creates cationic vacancies and oxidizes Co^{2+} to Co^{3+}. A low Co/Si atomic ratio on surface was found (Co/Si surface = 0.01) which indicated a low dispersion of Co_3O_4 over the SiO_2 support (Co/Si bulk = 0.11).

SEM analysis of Co10-c sample shows the presence of uniformed-size spherical formations of about 0.2 μm (Fig. 1a). Fig. 1b and c depicts higher magnification images. Some spherical aggregates deposited over the silica carrier are clearly visible in the backscattered electron image (Fig. 1c). Their sizes, up to 1 μm, are higher than those determined from XRD.

TEM analysis of the Co10-c sample (Fig. 2) shows a heterogeneous particle-size distribution of aggregates of cobalt oxide phase (0.1–1 μm).

During the activation of catalysts, cobalt oxides are reduced to metallic cobalt [24,27–30]. In order to study the structural changes that occur during the activation under different atmospheres, an in situ XRD study was carried during the treatment of Co10-c with H_2, CO or H_2 + CO from 298 to 773 K. Fig. 3 shows some of the XRD profiles obtained under the H_2 activation. The initial XRD pattern, which corresponds to Co_3O_4, is completely transformed at 548 K. At this temperature two main diffraction lines located at 36.5° and 42.5° appeared: they were assigned to CoO (1 1 1) and CoO

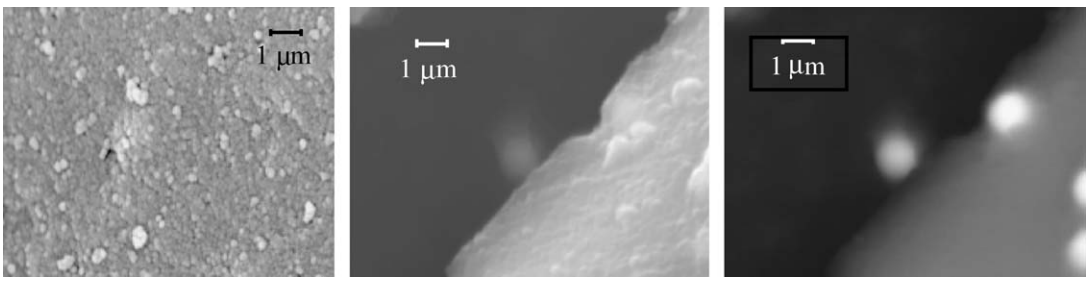

Fig. 1. Scanning electron microscopy images corresponding to Co10-c as prepared: (a) and (b) secondary electron images; (c) backscattered electron image.

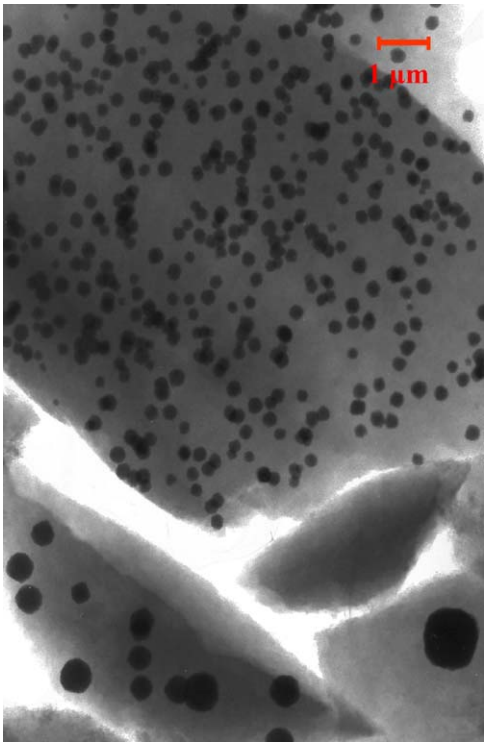

Fig. 2. TEM micrograph of Co10-c after calcination.

(1 0 0) diffraction lines. Then, an increase of temperature to 623 K produced the partial reduction of the CoO to metallic cobalt (see the Co10–H_2 (623 K) diffraction pattern in Fig. 3, peaks at 44.4° and ca. 51° correspond to Co_{fcc} (1 1 1) and Co_{fcc} (2 0 0) diffraction lines respectively). At 773 K only the most intense diffraction line Co_{fcc} (1 1 1) at 44.4° is visible. These results are consistent with the reduction of Co_3O_4 oxide in two stages [23–26]:

$$Co_3O_4 + H_2 \rightarrow 3CoO + H_2O \quad (1)$$

$$3CoO + 3H_2 \rightarrow 3Co^0 + 3H_2O \quad (2)$$

The characterization of the H_2-activated catalyst by TEM reveals a heterogeneous size and non-uniform distribution of cobalt particles (see Fig. 4). The Co/Si atomic ratio at the surface, determined by XPS, is 0.01. This value corresponds to that of the Co10-c sample, which indicates that the H_2 treatment does not affect the dispersion of cobalt-based phases.

Fig. 5 displays the in situ XRD study of the Co10-c precursor under CO atmosphere up to 773 K. Under CO the Co_3O_4 is transformed to CoO at a slightly higher temperature (598 K) than under H_2 (548 K). At 698 K a low intensity diffraction line centred at ca. 44° rises. Although it could be indicative of the formation of metallic cobalt, the presence of graphite deposits cannot be ruled out because the characteristic lines at ca. 42° and 44° could overlap those of CoO and Co^0 phases. Only after a treatment at 773 K under carbon monoxide is it possible to deduce the presence of crystalline phases of Co^0. Diffraction maxima at 41.6°, 44.3°, 47.3° and 51.2° point to the presence of both Co (fcc) and Co (hcp). On the other hand, under these conditions abundant graphitic deposits and minor amounts of

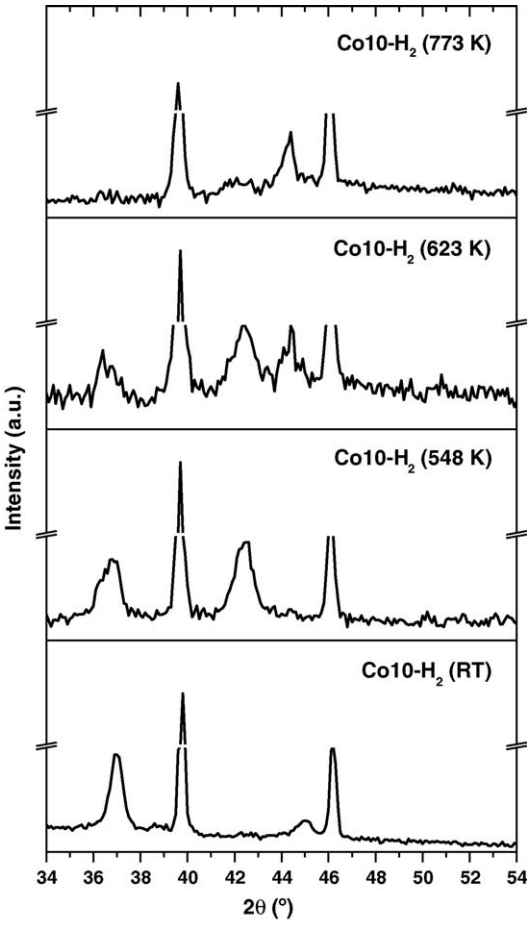

Fig. 3. In situ XRD patterns of Co10-c catalyst reduced in H_2 at different temperatures (Co10–H_2). Peaks at 39.6° and 46.1° are due to the platinum holder.

CoO are present, as deduced from the high intensity of the diffraction line at 44.3° and the very low intensity diffraction peaks at 36.5° and 42.5°. XPS analysis of Co10–CO activated at 773 K shows a Co/Si atomic ratio of 0.02, which is higher than that obtained after a H_2 treatment at the same temperature (Co/Si atomic ratio is 0.01 for Co10–H_2 (773 K)). Moreover,

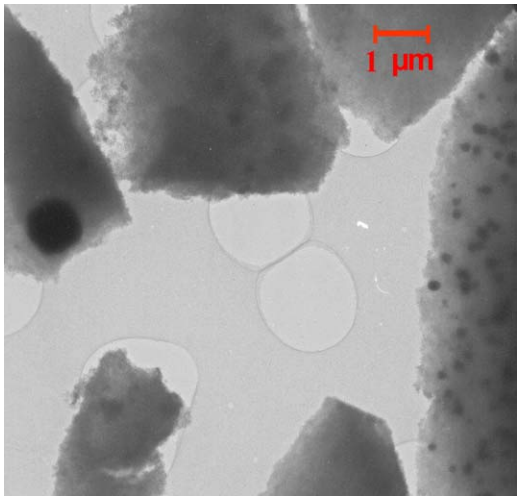

Fig. 4. TEM micrograph of Co10–H_2 (773 K).

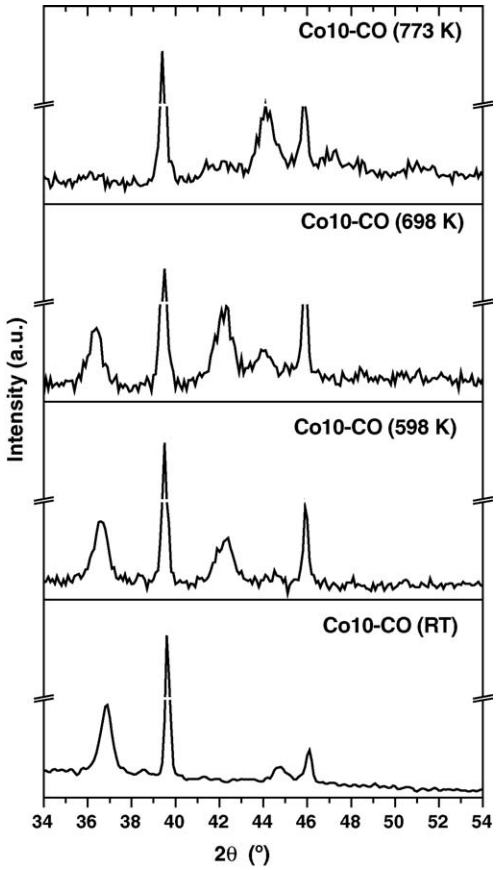

Fig. 5. In situ XRD patterns of Co10-c catalyst reduced in CO at different temperatures (Co10–CO). Peaks at 39.6° and 46.1° are due to the platinum holder.

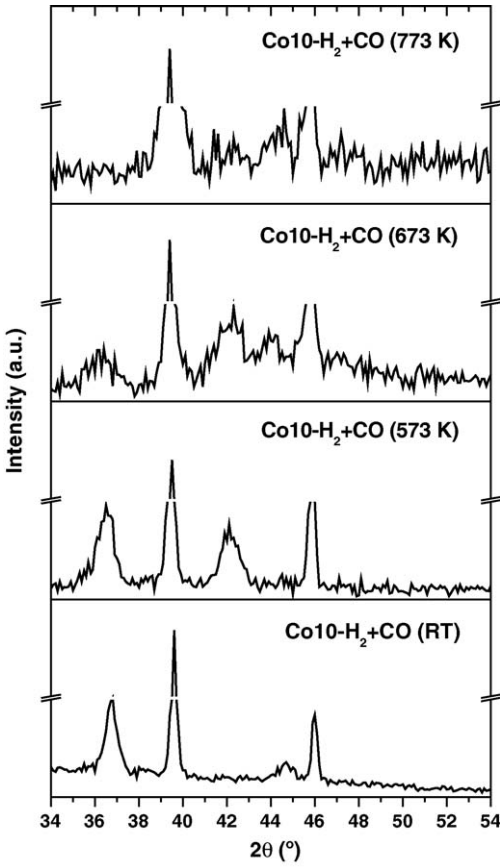

Fig. 6. In situ XRD patterns of Co10-c catalyst reduced in syngas at different temperatures (Co10–H_2 + CO). Peaks at 39.6° and 46.1° are due to the platinum holder.

after the CO treatment the intensity of the C 1s XPS signal increases strongly, coinciding with the XRD results. These results indicate an increase in metallic dispersion and a simultaneous increase in carbon deposits, which may be due to the Boudouard CO disproportionation:

$$2CO \rightarrow CO_2 + C\downarrow$$

The great amount of carbon deposits on the sample after the CO activation could explain the low performance of the sample in FTS if it is compared with the H_2-activated catalyst. However, the activity of syngas-activated sample has been demonstrated to be much higher than that of H_2-activated sample [20].

The in situ XRD analysis under syngas atmosphere is depicted in Fig. 6. Co_3O_4 is almost completely converted to CoO at 573 K. This is an intermediate temperature between the transformation of Co_3O_4 to CoO under CO (598 K) or under H_2 (548 K) (Figs. 3 and 5).

When the temperature increases to 673 K under H_2 + CO, the diffraction pattern exhibits broad maxima centred at 42°, 44° and 47°, which can reasonably be ascribed to the presence of Co (hcp) (diffraction lines at 41.7°, (1 0 0); 44.8°, (0 0 2) and 47.6°, (1 0 1)). However, at this temperature part of the CoO remains unreduced (peaks at 36.5° and 42.5°), further temperature increase produces its progressive disappearance.

After syngas activation above 673 K, the quality of diffraction patterns diminishes, probably due to the abundant carbon deposition and formation of carbon nanostructures, that produces an increase of the sample volume, and consequently a variation of its diffraction plane. However, at 773 K the

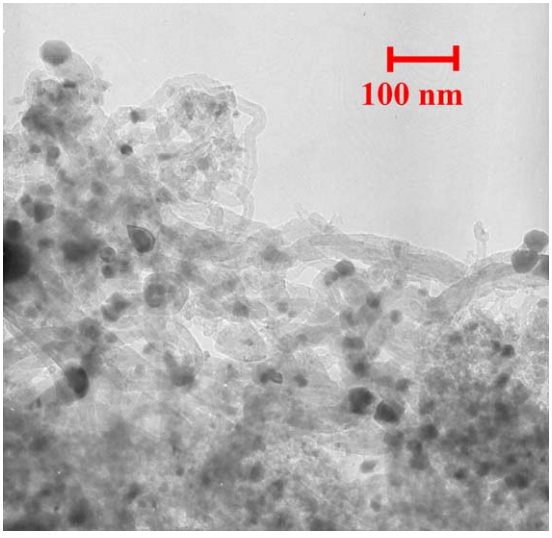

Fig. 7. TEM micrograph of Co10–H_2 + CO (773 K).

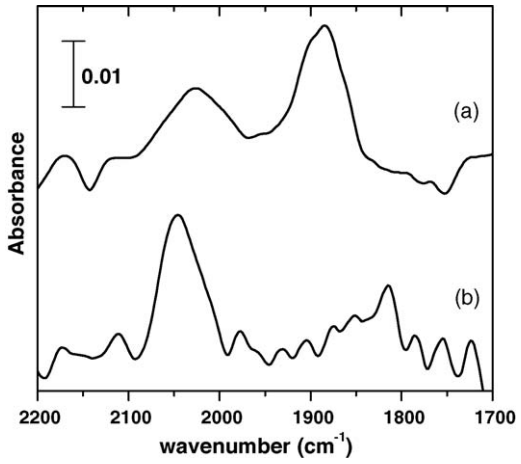

Fig. 8. DRIFT spectra in the υ(CO) region corresponding to: (a) Co10–H_2 + CO activated at 673 K and quenched under He to 298 K; (b) chemisorption of CO at room temperature over Co10–H_2 (673 K).

presence of Co (hcp) can be inferred (observed peaks at 41.6°, 44.7° and 47.3°). Fig. 7 shows a representative TEM micrograph of the Co10–H_2 + CO sample activated at 773 K, with large differences respect to the H_2-activated sample (Fig. 3). Homogeneously distributed cobalt particles, sized 30–80 nm, are dispersed in filamentous carbonaceous structures. According with the re-dispersion of cobalt under syngas, the XPS analysis shows an increase in the surface Co/Si atomic ratio. After syngas activation at 773 K, the Co/Si atomic ratio is six-fold that obtained after hydrogen treatment at the same temperature. Under syngas, the catalyst reduction is accompanied by the formation of carbon nanostructures, which is catalyzed by cobalt particles [31–33]. The cobalt reduction may be favoured by the presence of H_2 in the syngas, and the formation of carbon nanostructures would prevent the sintering of cobalt particles favouring their dispersion.

In order to complete the characterization of materials and evidence differences on chemisorption properties, in situ DRIFT-MS experiments were carried out. A sample was activated under flowing syngas up to 673 K in the spectrometer chamber and then, cooled down to 298 K under He. Fig. 8 depicts the corresponding spectrum (a) obtained at 298 K under He. It shows very broad bands with maxima at 2026 and 1884 cm^{-1}. Although the band located at 2026 cm^{-1} could be attributed to the presence of linear CO coordinated on metallic cobalt [34], the band at 1884 cm^{-1} cannot be straightforward assigned to the corresponding bridged chemisorbed CO on metallic cobalt particles. Moreover, an ulterior thermodesorption experiment, carried out in situ by increasing temperature from 298 to 373 K under He, showed the progressive and parallel disappearance of both bands. From this experiment it could be reasonably proposed the presence of $Co_x(CO)_y$ (x = 1–4, y = 4–12) surface species [35–37] which may be formed when Co_3O_4 is activated under syngas. In this respect, the formation of cobalt carbonyl clusters from CO treatment of small Co particles has already been proposed [37–40].

In a separate experiment the chemisorption of CO onto Co10–H_2 (673 K) was monitored by DRIFT. After an in situ treatment with H_2 at 673 K in the DRIFT chamber, sample was cooled under He to 298 K, exposed to helium-diluted CO and then flushed with He. The spectrum (b) in Fig. 8 was then recorded. Now, a main relatively broad band rose at 2045 cm^{-1}, which can reasonably be assigned to CO linearly-coordinated on reduced cobalt particles [34].

4. Conclusions

This study indicates the influence of the activation process on the structural and morphological characteristics of silica-supported cobalt catalysts. Silica- supported Co_3O_4 reduction to metallic cobalt proceeds differently depending on the reducing atmosphere. Under H_2 a heterogeneous size distribution of Co (fcc) particles is obtained. Homogeneously dispersed Co (hcp) nano-sized particles on carbon nanostructures are obtained under syngas activation. During the syngas activation cobalt carbonyl cluster species may be present.

Acknowledgments

This work was supported by Ministerio de Ciencia y Tecnologia (MCYT) (Spain) (MAT2001-2215-C03-01) and Generalitat de Catalunya (2005-SGR00184). VAPO acknowledge financial support from the MCYT in the Juan de la Cierva Program.

References

[1] F. Morales, D. Grandjean, F.M.F. de Groot, O. Stephan, B.M. Weckhuysen, Phys. Chem. Chem. Phys. 7 (2005) 568.
[2] H.P. Wither Jr., K.F. Elizer, J.W. Michel, Ind. Eng. Chem. Res. 29 (1990) 1807.
[3] R.C. Brady, R.J. Pettit, J. Am. Chem. Soc. 103 (1981) 1287.
[4] J.R. Anderson, P.S. Elmes, R.F. Howe, D.E. Mainwaring, J. Catal. 50 (1977) 508.
[5] M.A. Vanice, Catal. Rev. 14 (1976) 153.
[6] E. Iglesia, Appl. Catal. A 161 (1997) 59.
[7] M.E. Dry, Catal. Today 6 (1990) 183.
[8] R.C. Reuel, C.H. Bartholomew, J. Catal. 85 (1984) 78.
[9] K.E. Coulter, G.A. Sault, J. Catal. 154 (1995) 56.
[10] G. Jacobs, T.K. Das, Y. Zhang, J. Li, G. Racoillet, B.H. Davis, Appl. Catal. A: Gen. 233 (2002) 263.
[11] J. Panpranot, J.G. Goodwin Jr., A. Sayari, J. Catal. 211 (2002) 530.
[12] S. Sun, L. Fan, K. Fujimoto, Chem. Lett. (1999) 343.
[13] R.L. Chim, D.M. Hercules, J. Phys. Chem. 86 (1982) 370.
[14] R.L. Chim, D.M. Hercules, J. Phys. Chem. 74 (1982) 121.
[15] E. Iglesia, S.C. Reyes, R.J. Madon, S.T. Soled, Adv. Catal. 39 (1993) 221.
[16] B.G. Johnson, C.H. Bartholomew, D.W. Goodman, J. Catal. 118 (1991) 231.
[17] G. Bian, N. Fujishita, T. Mochizuki, W. Ning, M. Yamada, Appl. Catal. A 252 (2003) 251.
[18] H. Schulz, Z. Nie, F. Ousmanov, Catal. Today 71 (2002) 351.
[19] J.H. Wilson, G.R.M. Groot, J. Chem. Phys. 99 (1995) 7860.
[20] V.A. de la Peña O'Shea, J.M. Campos-Martin, J.L.G. Fierro, Catal. Commun. 5 (2004) 635.
[21] C.D. Wagner, L.E. Davis, M.V. Zeller, J.A. Taylor, R.H. Raymond, L.H. Gale, Surf. Interf. Anal. 3 (1981) 211.
[22] V.A. de la Peña O'Shea, N.N. Menendez, J.D. Tornero, J.L.G. Fierro, Catal. Lett. 88 (2003) 123.
[23] B. Ernst, S. Libs, P. Chaumette, A. Kiennemann, Appl. Catal. A 186 (1999) 145.

[24] B.A. Sexton, A.E. Hughes, T.W. Turney, J. Catal. 97 (1986) 390.
[25] D.G. Castner, P.R. Watson, I.Y. Chan, J. Phys. Chem. 94 (1990) 819.
[26] P. Arnoldy, J.A. Moulijn, J. Catal. 93 (1985) 38.
[27] K.E. Coulter, A.G. Sault, J. Catal. 154 (1995) 56.
[28] J.S. Girardon, A.S. Lermontov, L. Gengembre, P.A. Chernavskii, A. Griboval-Constant, A.Y. Khodakov, J. Catal. 250 (2005) 339.
[29] D.G. Castner, P.R. Watson, I.Y. Chan, J. Phys. Chem. 94 (1990) 819.
[30] D.I. Enache, B. Rebours, M. Roy-Auberger, R. Revel, J. Catal. 205 (2002) 346.
[31] A. Huczko, Appl. Phys. A 74 (2002) 617.
[32] J. Jiao, S. Seraphin, J. Phys. Chem. Solids 61 (2000) 1055.
[33] J.P. Pinheiro, M.C. Schouler, P. Gadelle, Carbon 41 (2003) 2949.
[34] N. Sheppard, T.T. Nguyen, in: J.C. Robin, R.E. Hester (Eds.), Advances in Infrared and Raman Spectroscopy, vol. 5, Wiley, 1978 (Chapter 2).
[35] R.L. Schneider, R.F. Howe, K.L. Walters, Inorg. Chem. 23 (1984) 4593.
[36] Y. Iwasawa, M. Yamada, Y. Sato, H. Kuroda, J. Mol. Catal. 23 (1984) 95.
[37] N. Homs, A. Choplin, P. Ramirez de la Piscina, L. Huang, E. Garbowski, T. Sanchez-Delgado, A. Théolier, J.M. Basset, Inorg. Chem. 27 (1988) 4030.
[38] J. Llorca, N. Homs, J. Sales, P. Ramirez de la Piscina, J. Mol. Catal. A 96 (1995) 49.
[39] J. Kiviaho, M.K. Niemelä, Y. Morioka, K. Kataja, Appl. Catal. 144 (1996) 93.
[40] J. Llorca, P. Ramirez de la Piscina, J.A. Dalmon, N. Homs, Appl. Catal. B: Environ. 43 (2003) 355.